Liquid Crystals Today

ISSN: (Print) (Online) Journal homepage: https://www.tandfonline.com/loi/tlcy20

Patterned surface alignment to create complex three-dimensional nematic and chiral nematic liquid crystal structures

Inge Nys

To cite this article: Inge Nys (2020) Patterned surface alignment to create complex three-dimensional nematic and chiral nematic liquid crystal structures, Liquid Crystals Today, 29:4, 65-83, DOI: 10.1080/1358314X.2020.1886780

To link to this article: https://doi.org/10.1080/1358314X.2020.1886780

Published online: 23 Feb 2021.

LIQUID CRYSTALS TODAY
2020, VOL. 29, NO. 4, 65–83
https://doi.org/10.1080/1358314X.2020.1886780

Taylor & Francis
Taylor & Francis Group

Patterned surface alignment to create complex three-dimensional nematic and chiral nematic liquid crystal structures

Inge Nys

LCP Group, Department of Electronics and Information Systems, Ghent University, Ghent, Belgium

ABSTRACT

Combining liquid crystals (LCs) with well-designed anchoring patterns at the substrates offers tremendous potential for the development of functional electro-optic devices or stimuli-responsive actuators. Photo-alignment techniques nowadays allow an almost arbitrary control over the surface anchoring and this flexibility is used to design highly efficient flat optical LC components with different functionalities. Part of this research, dealing with nematic and chiral nematic LC between substrates with patterned azimuthal anchoring, is reviewed here. The focus is on understanding the self-assembly of complex structures, steered by an interplay between surface anchoring and LC elasticity. Additional insight into the LC bulk behaviour is obtained by comparing experimental results with numerical simulations of the director configuration. Periodic anchoring patterns with azimuthal rotation at the top and bottom substrate are studied, as well as ring-shaped alignment patterns with a 180° or 360° azimuthal rotation in a confined region in space. Different combinations of anchoring patterns at the top and bottom substrates are investigated and in addition to nematic liquid crystal (NLC), also short and long-pitch chiral nematic liquid crystal (CLC) is considered.

KEYWORDS

Liquid crystal; photo-alignment; out-of-plane reorientation; flat optical components; director configuration

1. Introduction

Research on liquid crystals (LCs) ranges from fundamental science to applied research with practical applications in different domains [1–3]. The two most important features that make LC materials, with properties of both the liquid and the solid phase, so attractive are its anisotropy and tunability. The anisotropy of the molecular building blocks in combination with the long-range orientational ordering in the LC phase makes the macroscopic properties anisotropic. The strong responsiveness to external stimuli (electric field, magnetic field, heat, etc.), on the other hand, makes LC devices easily tunable. In rod-shaped thermotropic LCs, the average orientation of the long molecular axis is called the director **n**. The optical, electrical, magnetic and mechanical properties in the direction parallel to the director are different from those in the plane perpendicular to the director. Accurate control of the orientation of the director is therefore of crucial importance to manipulate the device characteristics.

After cell assembly, the director orientation can be actively controlled with external stimuli such as an applied electric field over the LC layer. This kind of voltage-induced director reorientation, and according to reorientation of the optical axis, is the key element for the immense success of LCs in the display industry over the last decades [4]. In LC displays the director alignment at the substrates is often uniform, but nowadays more and more attention is given to the use of patterned surface alignment to design LC components for novel applications [5–7]. A virtually unlimited number of alignment patterns can be used to define the director orientation at the substrates, leading to an immense flexibility to design LC components with the desired properties for the envisioned applications. Well-designed alignment patterns at the substrates can introduce complex LC structures in the bulk, especially when the patterning at the top and bottom substrates is different or when chiral liquid crystal (CLC) is used [8–14]. There is a lot of room to develop novel functional electro-optic LC devices or stimuli-responsive LC actuators [15,16] by using specifically designed alignment patterns at the substrates, in combination with appropriate LC materials. To successfully design these components, detailed knowledge of the self-assembly behaviour of the LC in the bulk is required. The LC configuration in the bulk is determined by a complex interplay between the surface anchoring and the LC elasticity (including possible chirality), and can be modified with the help of external stimuli. The complexity of the behaviour

CONTACT Inge Nys Inge.Nys@Ugent.be

strongly depends on the chosen alignment configuration at the surfaces and the type of LC material that is used, but numerical simulations for the director configuration are often indispensable to understand the device physics. This review article summarises recent work in this field conducted in the Liquid Crystals and Photonics Group at Ghent University. As mentioned before, the range of applications in this research domain is extended, but here we focus on patterned LC configurations to create so-called flat optical components, that are only a few micrometre thick but demonstrate excellent optical performance. Components such as beam splitters, lenses, diffraction gratings, lasers, etc. can be designed and offer tremendous potential for use in AR/VR devices, head-up displays, etc [5–11,17–30].

In this article, only cell geometries with two flat (non-curved) substrates are discussed. The substrates are coated with a transparent electrode (typically ITO) so that a voltage can be applied over the LC layer and different patterned alignment configurations at the substrates are investigated. There is a lot of literature in which only one photo-patterned substrate is used and one or multiple thin LC layers are spincoated and polymerised on top of that substrate [20,26,27]. In this case, there is only one patterned substrate, with limited control over the alignment at the (air) interface, and without the option to obtain reorientation by applying a voltage. This kind of spincoated LC layers will not be discussed further here.

To obtain a desired LC alignment pattern at the substrate, different techniques are available: micro-rubbing (for coarse alignment patterns) [31], lithography [32,33], ion-beam etching [34], self-assembled monolayers [35], and photo-alignment [36,37]. In the case of photo-alignment, a photo-sensitive alignment layer is deposited on top of the substrate and preferential alignment is induced with the help of polarised illumination. The focus in this article is on photo-alignment patterning whereby the azimuthal angle of the planar anchoring at the substrates is varied. This is the most commonly used technique to pattern the LC anchoring at the substrates, but alternative possibilities exist and can also lead to the creation of interesting LC structures in the bulk. To name a few examples, also patterning of the polar anchoring at the substrates (between planar and homeotropic) can be exploited as well as the introduction of surface topography. Patterning of the polar anchoring is usually more difficult to achieve than patterning of the azimuthal alignment. To do so, localised deposition of self-assembled monolayers was proposed [35], nanoimprint lithography [38], hard-contact photolithography with a chromium complex surfactant [39], or photo-alignment making use of a mixture of nanoparticles and azo-dyes in the LC [40]. We also reported on the use of a surface-based photo-alignment technique to induce a polar anchoring variation by combining a homeotropic alignment material with a conventional photo-alignment material [41]. Apart from chemical interactions between the LC material and the interface at the substrate, also surface topography is known to influence the LC anchoring [42–44]. This was mainly exploited in the past as an alternative for rubbing or photo-alignment to create planar LC anchoring along the surface grooves. We recently also demonstrated that when a lithographically patterned substrate with a well-chosen topographical period is combined with CLC, this can lead to voltage-induced directional growth of cholesteric fingers (long-pitch CLC) or a uniform lying helix-like (for short pitch CLC) structure [32,33]. This behaviour was not induced by the topography (height difference) of the surface, but rather by the difference in anchoring that is obtained for the ITO-coated areas and the areas covered by e-beam resist. Although very interesting, a more detailed discussion on these types of (polar) anchoring patterns and their effect on the bulk LC behaviour is outside the scope of this work.

As mentioned before, in this article we will focus on planar anchoring patterns with a variation in the azimuthal anchoring at one or on both substrates. The top and bottom substrate can be patterned with the same or a different pattern, or one substrate can be uniformly aligned (planar or homeotropic). In section 2 and 3 periodically rotating planar anchoring patterns will be discussed while (non-periodic) ring-shaped alignment patterns will be discussed in section 4. The experimental setups to define the anchoring patterns at the substrates are not discussed here in detail [11,45], but the patterning is based on photo-alignment. When linearly polarised UV or blue light is incident on a substrate coated with photo-alignment material (e.g. SD1, PAAD, Brilliant Yellow, etc.), the (azo-based) molecules in the alignment layer tend to reorient with their long axis perpendicular to the polarisation direction of the light [36,37]. Different illumination methods exist to create variations in the azimuthal anchoring at the substrate [7,17,46–48] and we use interference illumination or structured illumination with the help of a blue laser setup with a spatial light modulator (SLM). Alternative methods such as direct write illumination, plasmonic patterning, etc. have been reported in the literature and the preferred illumination method depends on the envisioned application.

2. One-dimensional periodic structures

The most commonly used photo-alignment pattern reported in literature is a periodically rotating planar alignment pattern with a 180° rotation of the azimuthal anchoring

direction over an alignment period Λ (Figure 1(a)). The director at the substrate (xy-plane) can be described by $n(\boldsymbol{x},\boldsymbol{y}) = \mathbf{sin}\left(\frac{\pi x}{\Lambda}\right)1_{\boldsymbol{x}} + \mathbf{cos}\left(\frac{\pi x}{\Lambda}\right)1_{\boldsymbol{y}}$.The alignment period Λ is typically varying from a few hundreds of nanometre to a few tens of micrometre, and the effect of this type of alignment pattern on different LC materials (NLC, CLC, dual-frequency LC, ferroelectric LC, etc.) was already investigated [10,19,49–51]. In this section, we describe two types of experiments in more detail: we focus on cells with the same periodically rotating alignment pattern at the top and bottom substrate (Figure 1(a), section 2.1) and briefly discuss the combination of a rotating alignment pattern at one substrate with uniform (planar or homeotropic) anchoring at the other substrate (section 2.2). In both cases the use of NLC and CLC is investigated.

2.1. Identical rotating anchoring at both substrates

2.1.1. NLC structures

The combination of NLC with a periodically rotating planar alignment pattern at both substrates (Figure 1(a)) was studied in great detail over the last two decades. The interest in these components was motivated by their tremendous potential for the development of so-called flat optical components (4th generation of optical components) that can achieve ideal phase surfaces (without Fresnel segmentation) with low cost manufacturing and high polarisation sensitivity [5–13,19–26,52,53]. In general, control over the wavefront direction in these type of components is achieved thanks to modulation of the optical axis orientation instead of the conventional modulation of the optical path length [52,53]. In the simplest assumption, the NLC director in the bulk simply follows the anchoring pattern at the substrates (Figure 2(a)), resulting in a patterned optical axis orientation that is uniform in the cell thickness. The patterned optical axis orientation is translated into a spatially varying geometric phase or so-called Panchara tnam Berry phase [54,55] and results in only three possible waves at the output of the LC layer (in the paraxial approximation): a primary wave, a conjugate wave and a leakage wave (0-order) [52,53]. The energy distribution in the three waves can be controlled between 0% and (nearly) 100% by adjusting the input polarisation state and the phase retardation in the LC layer. LC polarisation gratings (PGs) with close to 100% diffraction efficiency and modest driving voltages have been demonstrated in this way [53].

One of the limitations of NLC PGs is related to deviations of the ideal director configuration that appear in the bulk of the device. Uniformity of the director configuration along

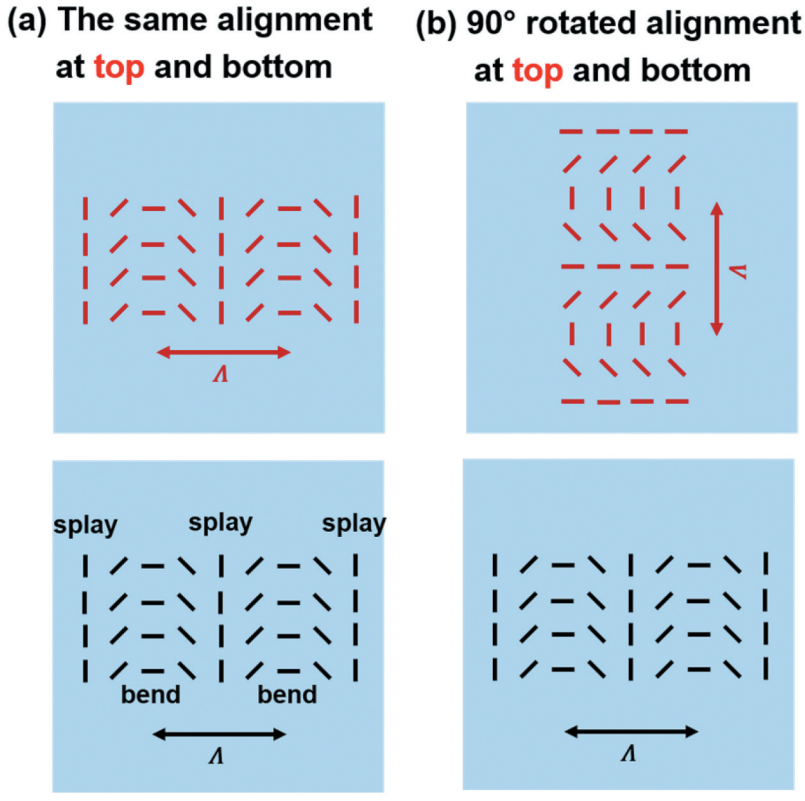

Figure 1. One-dimensional periodically rotating azimuthal alignment patterns defined at the top (red) and bottom (black) substrate. The same alignment at the top and bottom substrate is used in (a), while the periodic rotation direction at the top and bottom substrate is 90° rotated in (b).

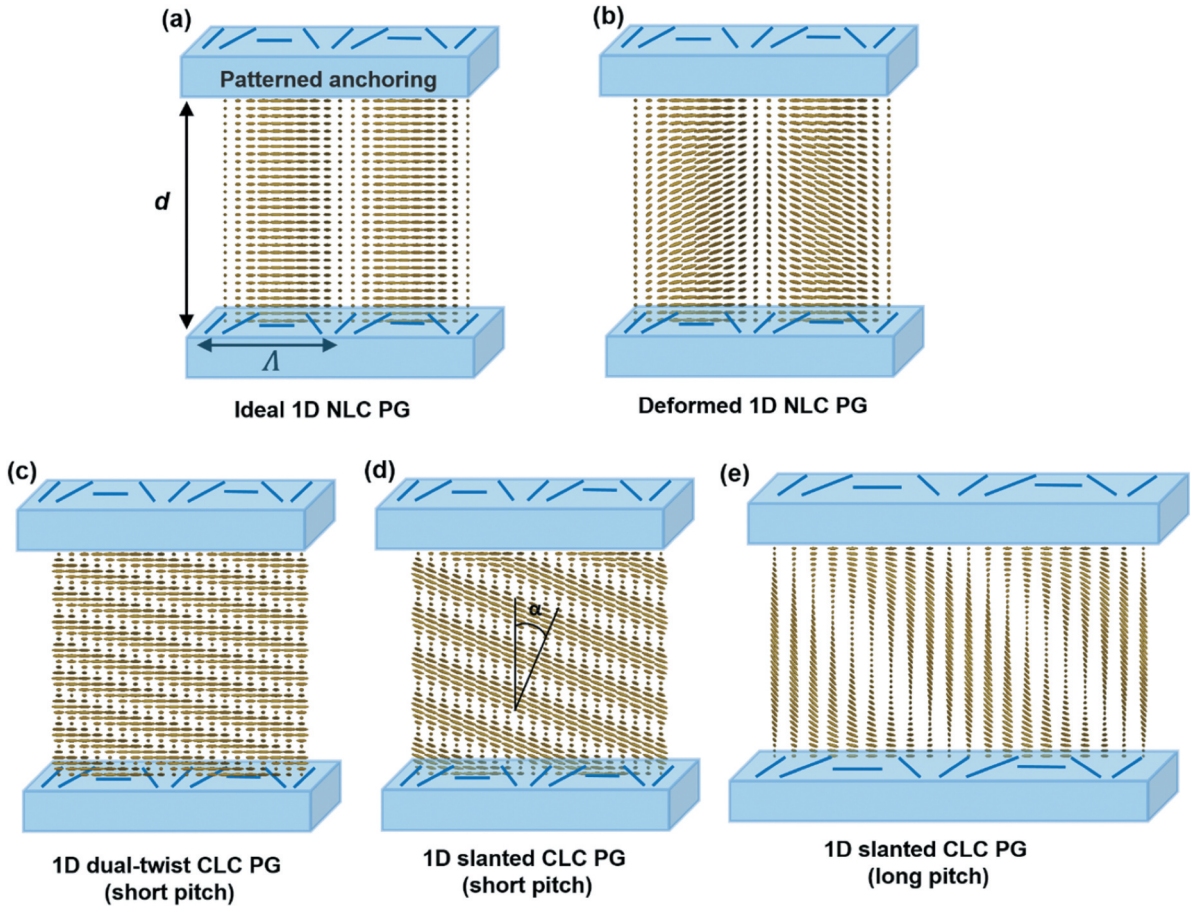

Figure 2. Schematic representation of some possible director configurations for NLC (a,b) and CLC (c,d,e) when infiltrated in a cell with the same periodically rotating azimuthal alignment at the top and bottom substrate. The actual director configuration might be more complex and will depend on *Λ, d, p* and the anchoring strength.

the z-axis, with the bulk director simply following the alignment pattern at the substrates (Figure 2(a)), is only achieved in good approximation in thin cells (w.r.t. Λ) with large anchoring strength. When the cell thickness *d* becomes comparable to the alignment period Λ, the NLC no longer follows the planar rotation but some out-of-plane reorientation of the director appears in the bulk (Figure 2(b)) [56]. This leads to deviations of the ideal behaviour and limits the maximal efficiency, especially when gratings with large diffraction angles (or lenses with large numerical apertures) are envisioned. The realisation of efficient LC-based optical axis gratings with a small period (or faster spatial variation) is therefore still a challenge. One approach that is followed in the literature to overcome the thickness limitation is to spincoat multiple thin LC layers on top of each other. This process is time-consuming, but fast optical axis variations can be obtained and lenses with a high numerical aperture have been demonstrated. Another interesting approach is based on the use of short-pitch CLC as will be discussed in the next section.

2.1.2. *Short pitch CLC structures*

Short pitch CLCs possess an intrinsic chiral periodicity that allows to support optical axis gratings with a short period and therefore empower the realisation of highly efficient reflective flat optical components with large steering angles. Patterning the spatial phase of the helical CLC structure, by applying non-uniform anchoring conditions at the substrate, allows to control the reflected wavefront [19]. The diffraction angle θ_{out} with respect to the substrate normal is related to the alignment period Λ and the wavelength of incident light λ by the grating equation $n_{out}\sin(\theta_{out}) = \frac{m\lambda}{\Lambda} + n_{in}\sin(\theta_{in})$ with *m* an integer number. The advantage of using short pitch CLC (instead of NLC) is that also very small alignment periods ($\Lambda < 500$ nm) and therefore large diffraction angles can be achieved. The working principle of these devices is based on Bragg reflection within the photonic bandgap of the CLC structure, and the director configuration in the bulk is more complex than in NLC PGs (no longer simply following the alignment pattern at the substrates, Figure 2). The interplay between

the alignment period Λ and the intrinsic chiral pitch p leads to a very rich behaviour that has attracted a lot of attention in the last few years [18,19,24,57–61].

We recently published an article in which highly efficient (88%), polarisation-sensitive, reflective diffraction over large angles (46° at λ = 633 nm, m = 1) was demonstrated in a 3 µm thick cell with Λ = 880 nm and p = 400 nm (Figure 3) [57]. The director configuration in the bulk of the device was simulated with the help of finite element modelling based on minimisation of the Landau-de Gennes free energy functional. In a follow up article we published optical simulations and transmission measurements under different angles of incidence for a similar cell with 5.5 µm thickness, Λ = 700 nm alignment period and p = 560 nm chiral pitch [58]. In these papers, we discuss the self-organisation of the chiral structure in the bulk, and the effect of the director configuration on the optical properties under different angles of incidence. Our work demonstrates that photo-alignment patterning at the surface with a period comparable to the chiral pitch, gives rise to the self-assembly of a tilted, defect-free helical structure as shown in Figure 2(d).

The underlying mechanism for the self-organisation into a slanted CLC configuration, with a tilted helical axis and a director that remains perpendicular to the helical axis in the bulk (Figure 2(d)), can be intuitively understood be considering the following arguments [57]. The rotating alignment pattern imposed at the surfaces contains a lot of splay and bend elastic energy (see Figure 1). The so-called dual twist director configuration or standing helix structure with variable helix phase (with tilt angle θ everywhere equal to 0°, see Figure 2(c)) that was previously proposed by others in literature [19,26–30], contains similar splay and bend elastic energy everywhere in the bulk and is therefore unfavourable in thick layers. However, by tilting the helical axis of the CLC away from the cell normal, the elastic energy in the bulk can become close to zero (unperturbed CLC structure) and in this case, only the transition region near the substrates contributes to the elastic energy. No energetically costly defects are required to match the anchoring conditions, and a smooth transition from the rotating surface alignment to the tilted CLC configuration in the bulk is obtained (Figure 2(d)).

Periodically rotating surface anchoring is in other words very well suited to stabilise a tilted CLC structure. Neglecting transition effects close to the substrates and the requirement for an integer number of chiral layers in a cell configuration, the slant angle α is related to the chiral pitch p and the alignment period Λ by $\sin(\alpha) = \frac{p}{2\Lambda}$. As explained in reference [58], the polar angle and azimuthal angle of the director can then be obtained based on spherical trigonometry formulae ([58], equation 4,5). Remark that this theoretical model can only be used to describe configurations with $p \leq 2\Lambda$. When the pitch becomes large (e.g. Figure 2(e)) compared to the alignment period, a transition towards more NLC-like behaviour can be expected and numerical simulations become indispensable.

For short-pitch CLC, transmission measurements under different angles of incidence that we recently published [58] allow to confirm the director configuration with a tilted helical axis, and demonstrate that a full reflection band can be observed for smaller angles of incidence than in standard planar CLC cells. Moreover, efficient forward diffraction for sufficiently large angles of incidence is demonstrated for the first time and the narrowing of the reflection band in CLC gratings due to total internal reflection is explained. The optical behaviour of a CLC grating with an inclined helix can roughly be understood by considering three layers: two linear gratings (near the top and bottom substrate) that are responsible for diffraction, and a homogeneous CLC layer in which only certain Bloch modes can propagate.

In general, these short-pitch CLC components with patterned surface anchoring offer interesting perspectives for the use in various flat optical components, combining high efficiency with the possibility for low-cost manufacturing at mass-production scale. Nowadays especially applications in the field of AR/VR systems are attracting significant attention and there are many efforts world-wide to further unlock the possibilities of thin-film LC components to achieve breakthroughs in this application domain. Although the basic principles behind photo-patterned CLC optical components are roughly understood today, there is still much room for improvement in the future. The design-freedom in developing photo-patterned LC components is still far from fully exploited and in-depth numerical simulations (taking into account finite anchoring energies, investigating the effect of different material parameters, etc.) are often still lacking. To fully optimise the optical performance of LC-based flat optical components, combined effort on material investigation, processing development and numerical simulation seems indispensable.

Other LC material systems, strongly deviating geometrical constraints (Λ, d, p) and the possibility for electrical tuning in helicoidal LC systems [62,63] in combination with photo-patterned anchoring, are some examples that are currently attracting our attention. As hinted before, strongly deviating device properties can simply be obtained by adjusting the spatial period A, cell thickness d and/or the chiral pitch p. These parameters determine the director configuration and the optical regime (Bragg, Raman-Nath, etc.) in which the components are working.

As an example, a possible director configurations for long pitch ($p \approx 5$ µm) CLC in a cell with roughly comparable alignment period and cell thickness ($\Lambda \approx d \approx p \approx 5$ µm) is sketched in Figure 2(e). Since the surface period, the pitch and the cell thickness are comparable, only a small number of chiral half pitches fits in the cell thickness. The director configuration can still roughly be interpreted in terms of tilted chiral planes and a helix axis that is tilted away from the cell normal, but the influence of the surface is larger and the helical structure is more deformed (requiring numerical simulations). This example already hints that in a specific geometrical regime, the director configuration can resemble a lying helix structure with the helix axis parallel to the substrates. This is one of the features that should be further investigated in the future.

2.2. Rotating anchoring at one substrate, uniform anchoring at the other substrate

2.2.1. NLC structures

In this section, we discuss the combination of periodically rotating planar alignment at one substrate with uniform (planar or homeotropic) anchoring at the counter substrate. This option was already considered by Crawford et al. [10] back in 2005 for (non-chiral) NLC cells and, as will be discussed in section 4., later on others also investigated the combination of non-period rotating azimuthal alignment with uniform planar alignment in NLC cells [64,65]. In general, this can lead to the creation of defect lines in the bulk of the NLC layer or induce out-of-plane reorientation of the director and possible symmetry breaking of the structure (see section 3 and 4). Even though the geometry and the NLC material system are rather simple, the resulting director configuration can be non-trivial and is not always correctly understood.

2.2.2. Short-pitch CLC structures

We recently also studied the infiltration of short-pitch CLC in cells with patterned planar alignment in combination with uniform homeotropic alignment [57]. We have shown that one photo-patterned substrate is sufficient to template the slanted CLC configuration as described in section 2.1.2., suited for efficient reflective diffraction. Close to the homeotropic substrate, large elastic energy is present and singular defects can be formed as seen in Figure 4(b). Remark that a non-singular transition from a chiral structure to a homeotropic background, as described in cholesteric fingers, is also possible and might be expected in long-pitch chiral systems [32].

Despite the fact that the transition from a tilted CLC structure towards a uniform homeotropic alignment is non-trivial, this alignment configuration also offers advantages. More specifically, the homeotropic counter substrate imposes less stringent requirements on the slant angle for the CLC structure: no integer number of chiral layers is required in the cell thickness as is the case in a cell with two photo-patterned substrates (section 2.1.2), so there will be no discrete jumps in the slant angle. We have already shown experimentally that, despite the presence of distortions, the top interface with strong homeotropic anchoring does not necessarily pose strong limitations on the diffraction efficiency in periodic CLC gratings [57]. This research is now being extended to cells with different thicknesses and with non-period alignment patterns.

3. Two-dimensional periodic structures

In this section the focus is on geometries in which the alignment is planar with periodically rotating azimuth, but the optical axis variation at the top and bottom substrates occurs along perpendicular directions as illustrated in Figure 1(b). Before the cell is assembled, one of the substrates is rotated over 90°, so that the alignment direction varies along the x-direction on the bottom substrate and along the y-direction on the top substrate. This type of surface alignment gives rise to the formation of a 2D periodic grating with a complex 3D LC structure in the bulk of the device. The LC configuration depends on the periodicity of the alignment Λ and on the thickness d of the cell.

Crawford et al. [10] in 2005 ($\Lambda = 15$ µm, $d = 5$ µm) and Provenzano et al. in 2007 [9] ($\Lambda = 20$ µm, $d = 3, 5, 7, 10$ µm) where the first to study crossed assembly of rotating planar alignment patterns and they proposed a simplified bulk structure with a position-dependent twist in the director configuration. As already hinted by Provenzano et al. [9], this simple picture of an ideal 2D twisted configuration (without out-of-plane reorientation) breaks down in many cases, especially when Λ/d becomes larger. Wang et al. [14] reported in 2017 that a similar combination of orientationally patterned substrates can be used to create a free-standing web of twist disclination lines. These twist disclinations were obtained in cells with $\Lambda = 53$ µm and d approximately 10 µm, when the cell was assembled by sliding a patterned substrate loaded with NLC, on top of the other patterned substrate at room temperature.

We, however, demonstrated in recent years for three different (Λ, d) combinations ((Λ, d) = (6.5 µm, 3 µm); (3.2 µm, 3 µm) and (12.5 µm, 10 µm)) that a defect-free director configuration, with strong out-of-plane reorientation of the director, is typically the minimal energy state in these types of cells with crossed assembly of rotating planar alignment surfaces [11–13]. When the

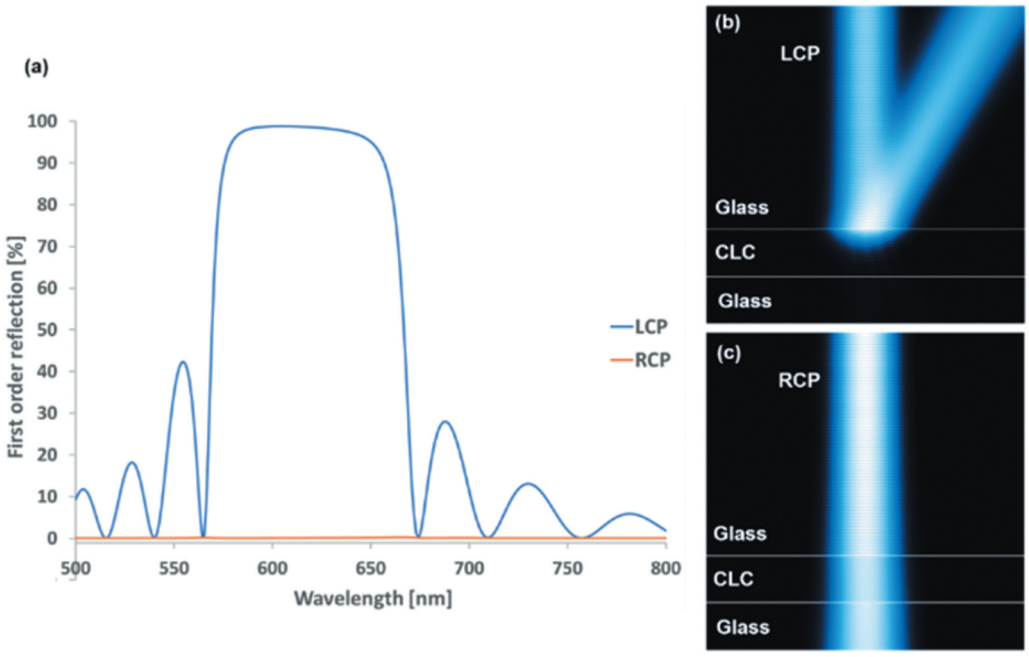

Figure 3. Numerically calculated first-order diffraction efficiency spectrum for left- and right-handed circularly polarised light (LCP and RCP) under normal incidence in a cell with two photo-aligned layers with $\Lambda = 0.88$ µm, $d = 3$ µm, and $p = 0.4$ µm. b,c) Simulated intensity distribution for a left-handed b) and right-handed c) circularly polarised Gaussian beam with wavelength $\lambda = 633$ nm [57]. The figure is re-used without modification from Figure 4 in reference [57] DOI: 10.1002/adom.201901364.

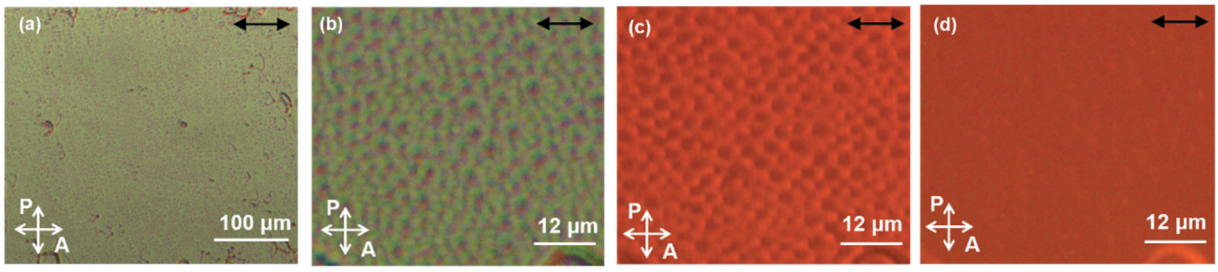

Figure 4. Polarising optical microscopy images in transmission (a,b) and reflection (c,d) with different magnification inside the photoaligned region of the cell with one photoaligned substrate and one homeotropic substrate, thickness d = 5.5 µm, chiral pitch p = 0.4 µm and period Λ = 1.1 µm. The difference between a and b is the scale of the image. The images in reflection (c,d) are taken with a red filter and the incident polarisation is right- and left-circularly polarised in c and d, respectively. The orientation of the grating vector is indicated with a black arrow. The figure is re-used without modification from Figure 2 (e-h) in reference [57] DOI: 10.1002/adom.201901364.

cell is filled at high temperature and cooled down to room temperature, this intricate director configuration with localised regions with vertical director configuration (Figure 5) is spontaneously formed. The surface-induced twist conflicts are elegantly resolved (without the need for singular disclination lines) by introducing regions with vertical director orientation in the bulk of the device. To find the complex 3D equilibrium director distribution we used finite element simulations based on Q-tensor theory [11–13]. The director configuration was then used to simulate the near-field transmission profile based on the Jones calculus and the diffraction properties were simulated with the help of a 2D Fourier transform. By comparing experimental measurements (microscopy, diffraction) the validity of the proposed director configuration was confirmed and this was repeated for different applied voltages to demonstrate the tunability of the components.

The results indicate that the LC forms a superstructure (unit cell 2Λ x 2Λ) with a lower periodicity than the configuration defined by the boundary conditions (unit cell Λ x Λ). This is reminiscent of symmetry breaking that

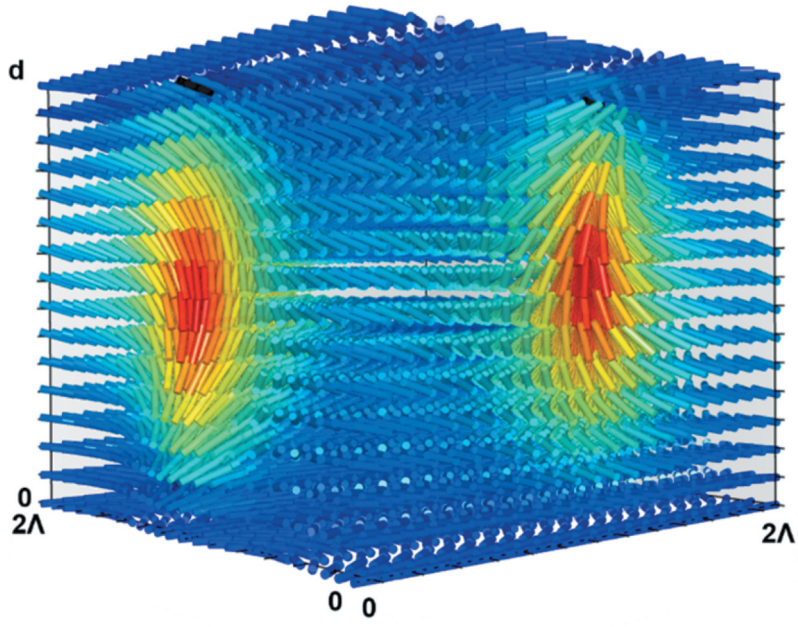

Figure 5. Simulated 3D director configuration in cells with crossed assembly of 1D periodically rotating alignment patterns at the top and bottom substrate. The colour represents the tilt angle, with the red colour indicating a close to vertical director orientation.

takes place in order to avoid the formation of disclinations and to reduce the total free energy in the director configuration. Such a possibility was often overlooked in previous literature [9,10,14] but we could convincingly demonstrate symmetry breaking, leading to a disclination-free director configuration with 2Λ by 2Λ unit cell and out-of-plane tilt of the director. The mechanism to avoid a twist conflict by introducing an out-of-plane tilt of the director, can also be used in more general conditions to design non-periodic topological entities with a localised out-of-plane director orientation as will be discussed in section 4.

3.1. NLC structures with different dimensions (Λ, d)

In general, when a different azimuthal angle is imposed at corresponding locations at the top and bottom substrate, in a simplified picture one could expect that a position-dependent director twist in the bulk would occur (as proposed in [9,10]). However, for the 90° rotated orientation of alignment patterns at the substrates (Figure 1(b)), the topology at the interfaces requires either the creation of disclinations in the bulk or regions with vertical director orientation [11–14]. To make this intuitively clear, Figure 6 graphically represents the directors for one specific cross-section on the unit sphere. In the cross-section with

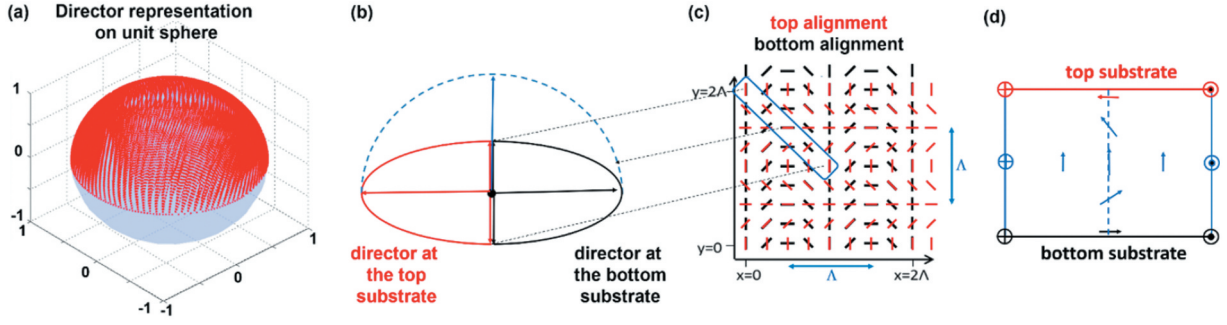

Figure 6. Alignment at the top and bottom surface (c) together with a graphic representation of the directors in a cross-section on the unit sphere (a) and a schematic representation of the top and bottom alignment in this cross-section (b,d). The cross-section is taken between the corner points (0, 2 Λ, 0), (0, 2 Λ, *d*), (Λ, Λ, 0), (Λ, Λ, *d*) as indicated with the blue rectangle. The alignment at the top and bottom substrate describes a half circle in the equatorial plane, the director in the bulk fills the half unit sphere.

corner points (5/4 Λ, 5/4 Λ, 0), (5/4 Λ, 5/4 Λ, *d*), (9/4 Λ, 1/4 Λ, 0), (9/4 Λ, 1/4 Λ, *d*) the alignment at the top and bottom surface describes a half circle in the equatorial plane (rotation 180°) but in opposite directions. As a result, a twist disclination is unavoidable if the director stays parallel to the substrates everywhere in the bulk. A director configuration that includes a vertical orientation in the bulk, allows to fill the half unit sphere without a discontinuity (Figure 6(a)).

This out-of-plane tilting of the director (to avoid twist disclinations) is inherently linked to the symmetry breaking that we observe in these 2D NLC gratings. In the 2Λ by 2Λ unit cell for the director configuration (Figure 5, 8), four different equivalent positions exist, shifted horizontally and/or vertically over a distance Λ. Different domains with shifted gratings may therefore be observed in the photo-aligned region as shown in Figure 7. These domains are separated by a defect line.

To further investigate the complex director configuration we compared cells with different alignment period Λ and cell thickness *d* combinations: (Λ, *d*) = (6.5 µm, 3 µm); (3.2 µm, 3 µm); (12.5 µm, 10 µm), and applied external voltages [11–13]. In all cases, a stable and in general defect-free LC structure was obtained with a 2 Λ by 2 Λ unit cell (Figure 8). When a voltage is applied to the cell, the degree of vertical alignment in the bulk increases. At high voltages, the director is oriented vertically in the bulk and the retardation close to the substrates is small. At positions with a parallel director orientation at the top and bottom substrates, some transmission is observed if this orientation is under an angle with the polariser and the analyser (Figure 9). If the directors at the top and bottom substrates are oriented perpendicularly, the transmission is low since the retardation near the top and bottom substrate have an opposite sign and compensate each other (Figure 9).

In general, changing Λ and *d* individually while conserving the Λ/*d* ratio will not influence the director configuration since the elastic energy is scaled proportionally. This holds in the assumption of strong anchoring

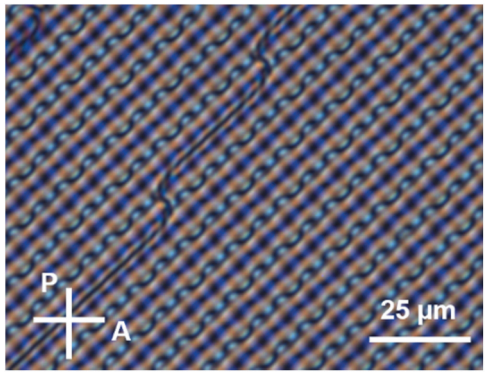

Figure 7. Polarising optical microscopy image for a cell (Λ = 6.5 µm, *d*= 3 µm) with crossed assembly of 1D periodically rotating alignment patterns at the top and bottom substrate (Figure 1 (b)). Shifted domains can be observed, separated by a defect.

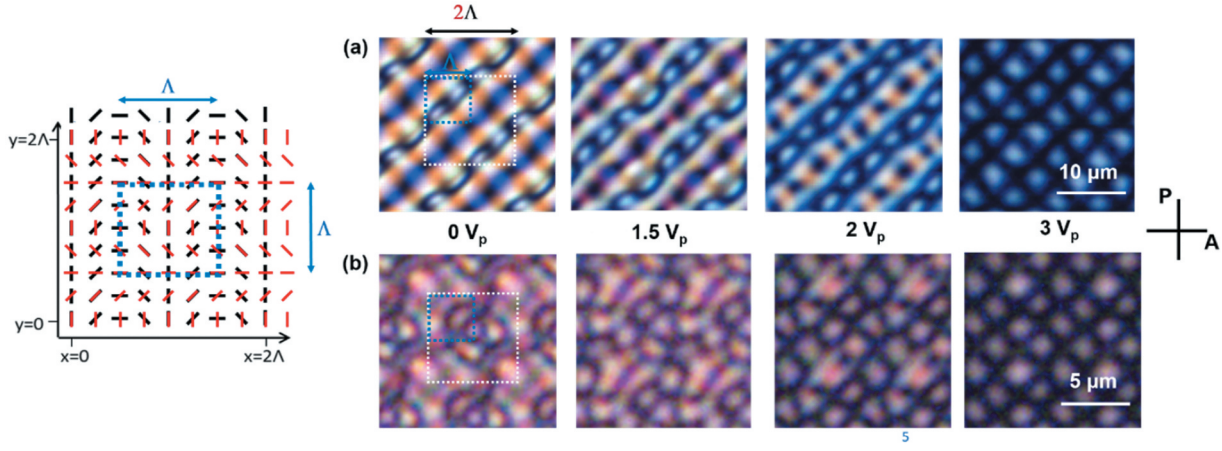

Figure 8. Polarising optical microscopy images at different applied voltages (V_p = peak voltage) for cells with crossed assembly of 1D periodically rotating alignment patterns at the top and bottom substrate [11,12]. (Λ, *d*) = (6.5 µm, 3 µm) in (a) and (3.2 µm, 3 µm) in (b). Reproduced from Ref [11]. and Ref [12]. with permission from the Royal Society of Chemistry.

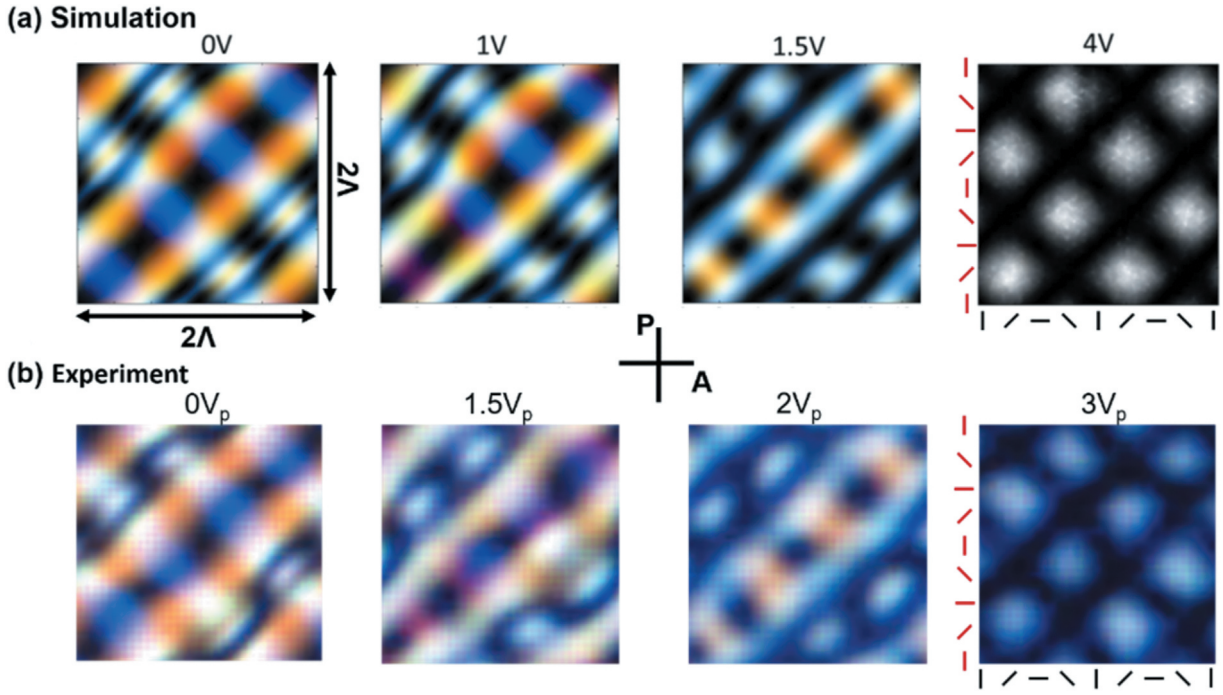

Figure 9. Comparison between the simulated (a) and experimentally measured (b) microscopy images in a cell with crossed assembly of 1D periodically rotating alignment patterns at the top and bottom substrate, with (Λ, d) = (6.5 µm, 3 µm). RMS values are reported in the simulations, peak values V_p are reported in the experiments. Reproduced from Ref [11]. with permission from the Royal Society of Chemistry.

conditions, but may break down experimentally in cells with a very small grating period since the finite anchoring energy has to be taken into account. In a first comparison, we did not change the cell thickness (d = 3 µm), but only decreased the alignment period (Λ = 3.2 µm instead of 6.5 µm) to investigate how a decreasing Λ/d ratio influences the director structure [11,12]. Differences between both configurations (with two times larger Λ/d ratio), are not related to the topology of the structure but to the exact values of the local twist angles and especially the local tilt angles in the bulk of the cell (Figure 10). In cells with a large Λ/d ratio the director orientation in the diagonal cross-section (x = y) is rather planar (tilt angle close to 0°) while it becomes more and more tilted for decreasing Λ/d ratios. Note that the director tilt in the diagonal cross-section is however not increasing homogeneously, with a more strongly tilted region around (Λ/4, Λ/4, d/2) in Figure 10. This is driven by a minimisation of the elastic energy and depends on the relative values of the elastic constants for splay, twist and bend.

The fact that the asymmetry in the unit cell becomes larger for cells with a smaller Λ/d ratio can also be seen in the experimental results (Figure 8) and was confirmed by the results that we reported in 2020 for an approximately three times thicker cell (Λ, d) = (12.5 µm, 10 µm) [13]. In that paper, we also investigated the director configuration experimentally with the help of oblique illumination and we focused on the effect of symmetry breaking on the possibility to form domains with different equivalent structures in the cell (two equivalent director configurations that can both be located at four equivalent positions in the unit cell).

To conclude, the director configurations for the investigated (Λ, d) combinations ((Λ, d) = (6.5 µm, 3 µm); (3.2 µm, 3 µm) and (12.5 µm, 10 µm)) are closely related to each other and the topology can be continuously transformed between them. Distinct topological configurations could be obtained by larger changes of the dimensions. Further decreasing the Λ/d ratio will lead to a close to vertical director orientation in the bulk, also at low voltages. In thin cells with a large Λ/d ratio on the other hand, twist disclination can be expected in the director configuration if the anchoring strength is strong enough. These twist disclinations can also be obtained in cells with smaller Λ/d ratio in non-equilibrium conditions [14]. In general, a plethora of new, highly periodic, LC structures can be obtained by varying the dimensions, the alignment pattern, and the LC that is used. The fact that symmetry breaking leads to structures with a larger period, indicates that inherently equivalent stable states

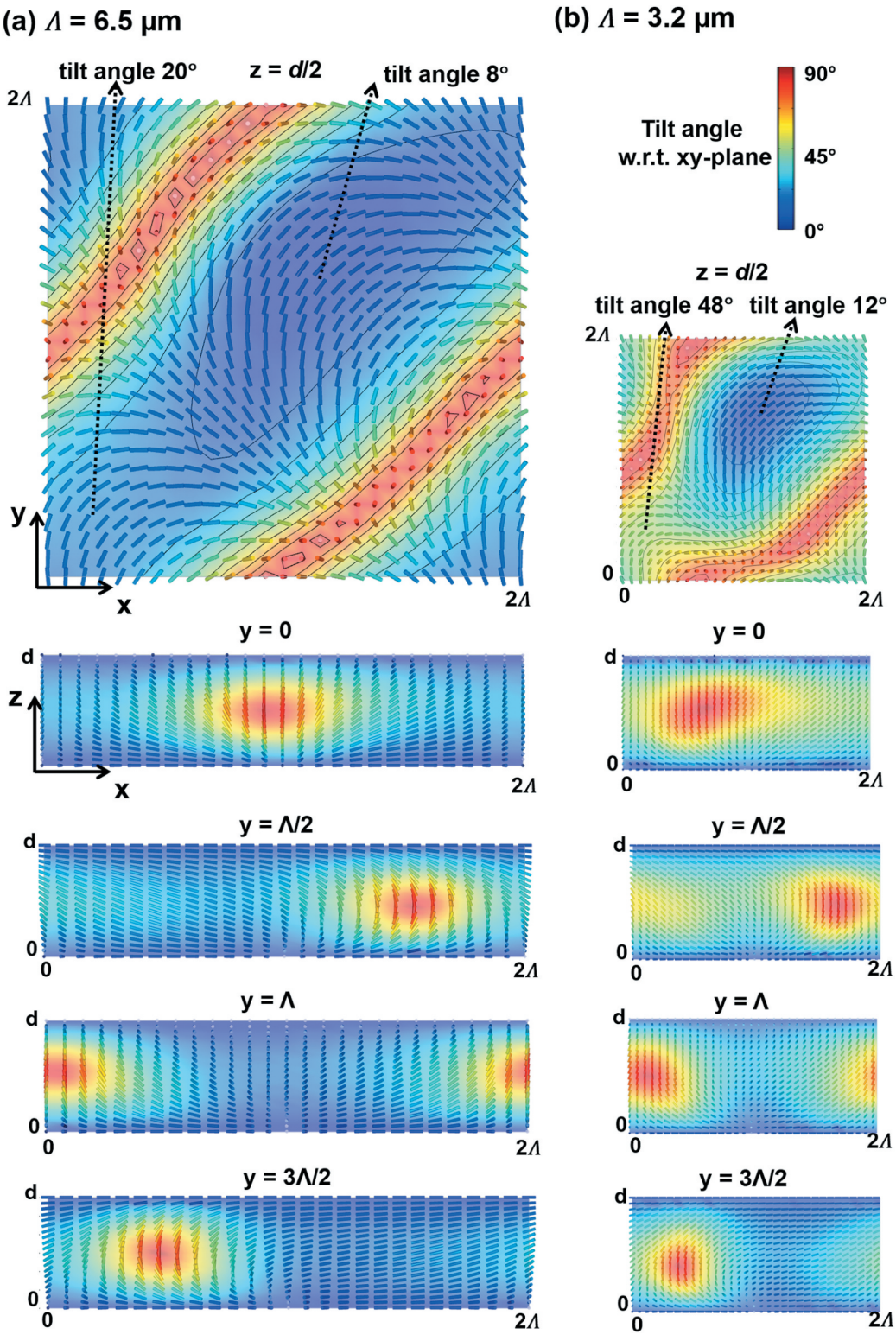

Figure 10. Simulated director configuration at 0 V in cells with crossed assembly of 1D periodically rotating alignment patterns at the top and bottom substrate (Λ, d) = (6.5 μm, 3 μm) in (a) and (3.2 μm, 3 μm) in (b). Partly reproduced from Ref [11]. and Ref [12]. with permission from the Royal Society of Chemistry.

and electro-optic devices with bistable behaviour could be obtained. It remains therefore worthwhile to study different combinations of cell geometry (*A, d*) and LC material (with and without chirality) in the future.

3.2. NLC structures with adjusted anchoring conditions

For completeness, it should be mentioned that we did not only perform the analysis of these 2D NLC gratings inside the normal grating area with strong photo-alignment at both substrates, but also in transition regions were one (or both) substrates was only weakly illuminated [12]. It was experimentally demonstrated that the strength of the illumination at both substrates can strongly influence the director configuration in the bulk of the cell. In regions with weak illumination at the top and/or bottom substrate, new structures with different symmetry properties are stabilised [12]. Areas with line patterns (area B in Figure 11) and waffle patterns (areas C1 and C2 in Figure 11) were experimentally observed and studied with the help of numerical simulations. In the areas with line patterns, the director fully rotates on one substrate (as a function of one coordinate), but oscillates around a mean value on the other substrate (as a function of the other coordinate). In the region with waffle patterns, both the alignment at the top- and bottom-interface oscillates around a mean value. Also for these regions with reduced asymmetry in the anchoring conditions, the 3D LC director configuration and the 2D transmission images were successfully simulated.

4. Soliton structures obtained by ring-shaped alignment patterns

In sections 2 and 3 we discussed the use of periodically rotating alignment patterns (Figure 1), leading to 1D or

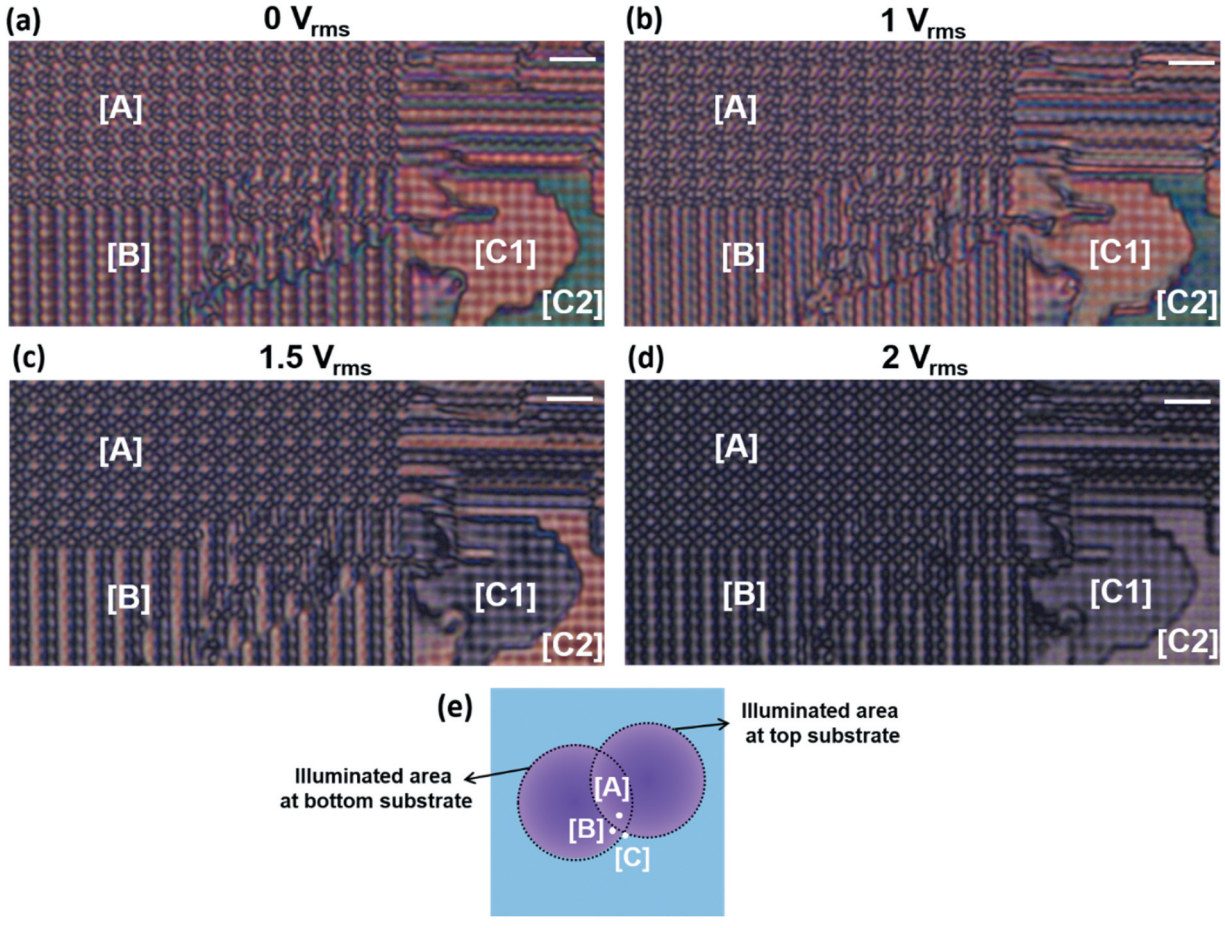

Figure 11. Polarising optical microscopy images for a cell (Λ = 3.2 µm, d = 3 µm) with crossed assembly of 1D periodically rotating alignment patterns at the top and bottom substrate, for four different voltages at the edge of the photo-aligned area; 0 V (a), 1 Vrms (b), 1.5 Vrms (c) and 2 Vrms (d). Three distinct regions, labelled A, B and C, can be recognised. The scalebar in figures (a–d) has a length of 10 µm. The position of the three different regions with respect to the illuminated area at the top and bottom substrate is schematically illustrated in (e). Reproduced from Ref [12]. with permission from the Royal Society of Chemistry.

2D periodic LC gratings. In this section, we will investigate alignment patterns with a non-periodic variation in the planar anchoring but with a modification of the azimuthal anchoring only in well-defined regions in space [45,64–67]. To do so, we exploit the flexibility of an SLM-based photo-alignment setup to define custom-designed patterns at the substrates [45,65]. Specifically, we here focus on ring-shaped alignment patterns with a 180° or 360° azimuthal rotation between the inner and the outer ring (Figure 12) [45,65]. Different dimensions for the inner radius r_{in} and the outer radius r_{out} were tested, but typical values are r_{in} = 20 µm and r_{out} = 50 µm (cell thickness $d \sim 5$ µm). Compared to finite line segments, ring-shaped patterns have the advantage that they have no start and end point and therefore do not require point defects to terminate the structure. Moreover, the ring-shaped alignment patterns can be used in an elegant way to stabilise topological solitons in NLC cells [45,65]. Solitons are very robust since they are localised and stable optical axis patterns which cannot be continuously deformed into a uniform orientational field. These particle-like topological states are usually studied in chiral LC samples with strong confinement [68–70], but photo-alignment techniques allow to generate soliton structures in less confined configurations [41] and non-chiral cells [45,64,65,67]. We here discuss soliton-like structures that can be obtained in cells with one patterned substrate (section 4.1., Figure 12(a)) or with two patterned substrates (section 4.2., Figure 12 (b)). The stabilised defect-free structures offer interesting opportunities for the use in waveguiding devices, optical switches and soft actuators. The twist-conflict induced by the anchoring patterns at the surfaces is typically resolved by the creation of a ring-shaped region with vertical director orientation in the bulk, without the need for singular disclinations [45,65]. This concept was already introduced in section 3 for rotated periodic anchoring patterns at the substrates and the same mechanism occurs in cell with ring-shaped alignment patterns [11–13].

4.1. Ring-shaped region with 360° azimuthal anchoring rotation on one substrate

In the first configuration, a ring-shaped alignment pattern with a 360° azimuthal rotation is present on one of the cell substrates, while the counter substrate is uniformly planar aligned (Figure 12(a)). The inside ($r < r_{in}$) and outside ($r > r_{out}$) of the patterned ring contain the same planar alignment as the one that is present at the counter substrate. We experimentally demonstrated that this alignment configuration can give rise to four different metastable LC structures in the bulk of the device and

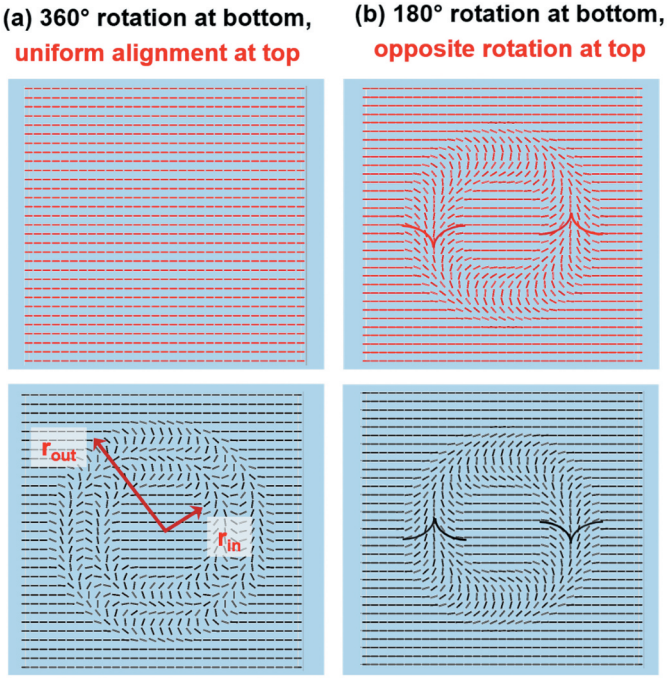

Figure 12. Ring-shaped photo-alignment patterns with an azimuthal rotation between r_{in} and r_{out}. In configuration (a) only the bottom substrate (black) is patterned with an azimuth that rotates over 360° between r_{in} and r_{out}. In configuration (b) both the top (red) and bottom (black) substrate are patterned with a 180° azimuthal rotation with opposite sense at both substrates.

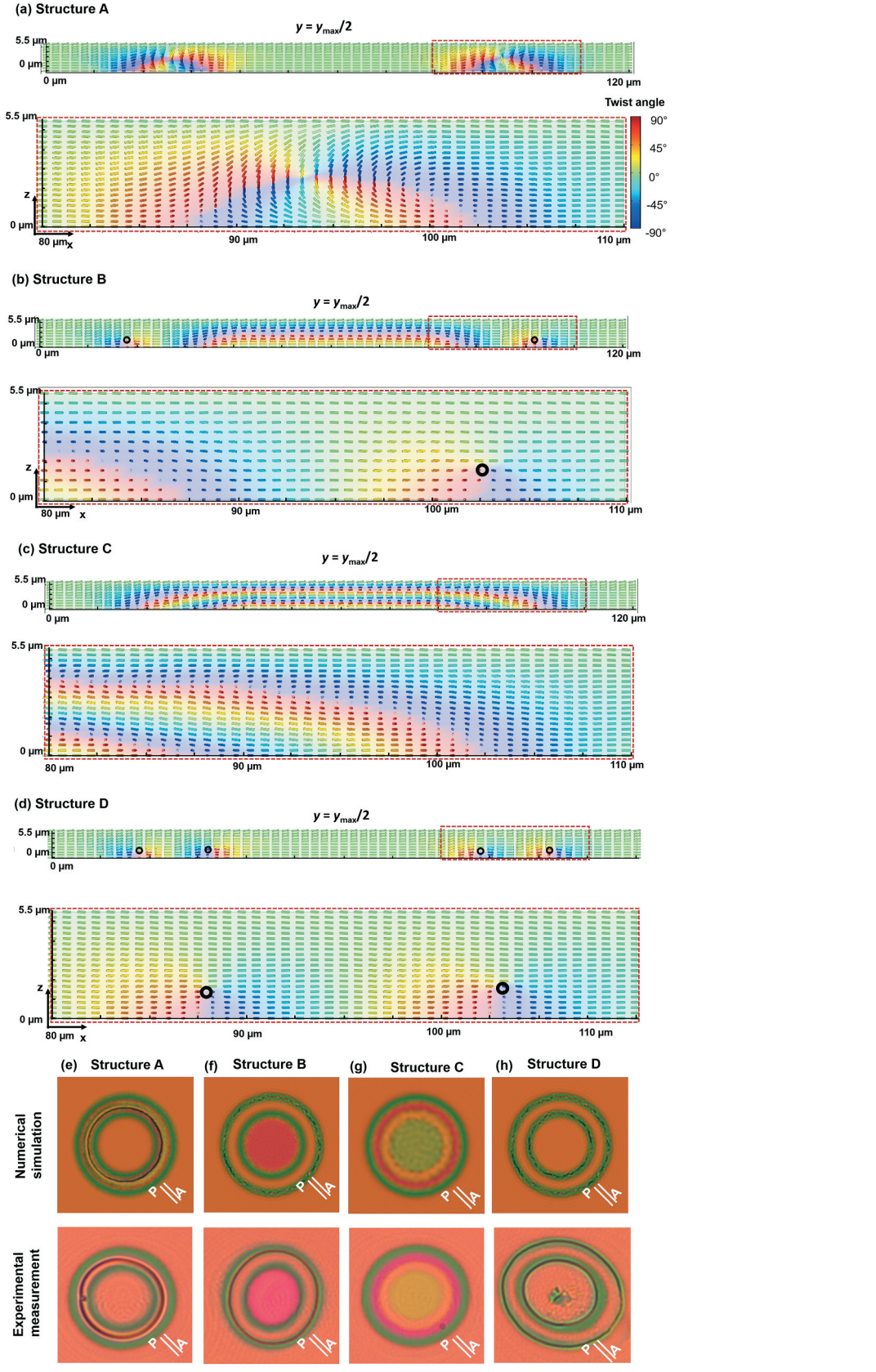

Figure 13. Simulated director configuration (a-d) and optical transmission (e-f) for structure A (a, e), B (b, f), C (c, g) and D (d, h) without applied voltage. The colour represents the twist angle with respect to the x-axis. The director configurations in a perpendicular cross-sections $y = ymax/2$ are shown. The defects in the director configuration are indicated by a black circle. The simulated microscopy images are compared to experimental microscopy images in (e-h). Reproduced from Ref [45]. with permission from the Royal Society of Chemistry. Parts of figures 9, 6 and 10 in Ref [45]. are selected.

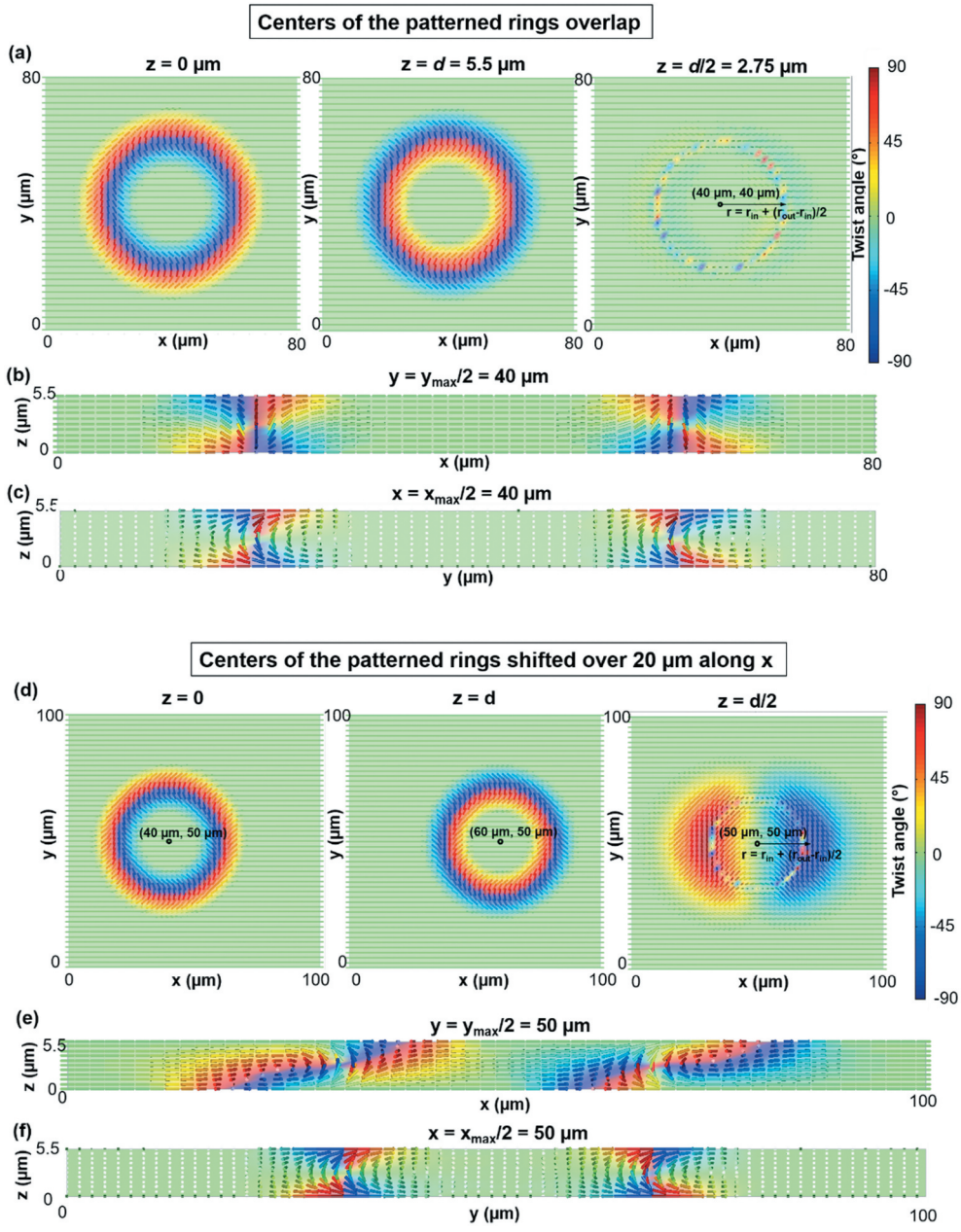

Figure 14. (a-c) Simulated director configuration for a configuration with perfect overlap between the centres of the patterned rings at the top and bottom substrate (80 µm x 80 µm x 5.5 µm unit cell, r_{out} = 30 µm, r_{in} = 0.4 * r_{out}). (d-f) Simulated director configuration for a configuration with a 20 µm shift between the centres of the patterned rings at the top and bottom substrate (100 µm x 100 µm x 5.5 µm unit cell, r_{out} = 30 µm, r_{in} = 0.4 * r_{out}). The colour represents the twist angle with respect to the x-axis. The director configuration is shown at the bottom substrate, the top substrate and the mid-plane z = d/2 (a, d), and in two perpendicular cross-sections y = y_{max}/2 (b,e) and x = x_{max}/2 (c,f). The figures are reproduced from figures 7 and 9 in reference [65].

successfully unravelled the director configurations with the help of numerical simulations [45]. The four structures were named structure A, B, C and D (Figure 13) and in essence their difference lies in the presence (or absence) of disclinations and the presence of a strong twist in the inner region ($r < r_{in}$) of the ring-shaped pattern.

Structure A contains no twist disclinations and no twist in the inner, unpatterned region of the ring (Figure 13(a)). The twist conflict at the top and bottom substrate is resolved by introducing an out-of-plane orientation of the director in the bulk, similar to what was discussed in section 3. This defect-free configuration with localised regions with vertical director orientation is very stable against voltage cycling (for LC with $\Delta\varepsilon>0$) and offers interesting opportunities for waveguiding applications. When a voltage cycle is applied to the

cell, structure A is dominantly observed after turning of the voltage.

The other structures (B, C, D) do not contain a region with vertical director orientation in the bulk, so based on the same arguments as in section 3 (Figure 6), one would expect that two twist disclination rings should appear in the bulk, one for every 180° azimuthal rotation at the bottom substrate (Figure 12(a)). This configuration is indeed observed (named structure D, Figure 13(d)) from time to time, but two other structures are seen as well. The possibility to form structure B and C (Figure 13 (b) and (c)), without vertical director orientation and with no (structure C) or only one (structure B) disclination ring, is inherently linked to the ring-shaped pattern of the alignment configuration. Since the alignment pattern has the form of a closed ring, the twist conflict at the top and bottom substrate can be resolved by introducing a bulk twist in the unpatterned inner region of the ring ($r < r_{in}$). One of the twist-disclinations can shrink and disappear, by introducing a 180° twist (in the z-direction) in the inner region of the ring (structure B). Additionally also the second disclination ring can shrink by introducing another 180° twist in the inner region of the ring, resulting in a configuration with 360° planar rotation between the top and bottom substrate for $r < r_{in}$ (structure C). In this case, we obtain a defect-free director configuration without introducing a region with vertical director orientation in the bulk. This comes at the cost of introducing a twisted region inside the ring pattern, so it is clear that the relative stability of the different structures (A, B, C, D) will depend on the exact geometry (r_{in}, r_{out}, d) and the used LC material (non-chiral, chiral, different elastic constants, etc.). Also the history of the sample (voltage treatment, heating cycle, etc.) and the exact alignment properties (alignment strength, pretilt, etc.) will influence the stability of the different structures. This is worth to be investigated further since the different structures have different optical properties and these kind of devices could be used in smart windows, multistable microlenses or displays with low energy consumption.

4.2. Ring-shaped regions with 180° azimuthal anchoring rotation at both substrates

In this configuration, the photo-aligned background at both substrates is uniformly planar aligned along the x-direction, but closed ring-shaped regions with a 180° rotation of the azimuthal angle (between r_{out} and $r_{in} = 0.4 * r_{out}$) are patterned at the top and bottom substrate (Figure 12(b)). The 360° azimuthal rotation at one substrate as discussed in the previous section 4.1 (Figure 12(a)), is here replaced by two times a180° rotation at the top and bottom substrate. In the ring-shaped patterns at both substrates, the azimuthal angle is rotating with an opposite sense of rotation (Figure 12(b)). This alignment configuration again leads to twist-conflicts, and in this case, only one stable director configuration is observed experimentally [65]. A configuration with two twist disclination rings of strength ½ (one connected with the top and one with the bottom substrate) is never encountered. Experiments and simulations demonstrate that a defect-free soliton structure, with a ring-shaped region with vertical director orientation, is formed in the NLC cell when the alignment rings at both substrates at least partially overlap (Figure 14). The topological structure formed in the bulk is inherently stable upon voltage cycling and is not easily destroyed by deviations in the anchoring configuration.

Remark that, since alignment patterns are present at the top and bottom substrates, both have to be carefully positioned with respect to each other. To have at least some positions in the cell where the centres of the rings overlap, we use the concept of lucky alignment: arrays of ring patterns are written at the top and bottom substrates, with slightly different spacing. Experimental results demonstrate that, thanks to the topological stability, a localised vertical director orientation in the bulk is also observed when the centres are shifted over relatively large distances (Figure 14(d-f)).

Compared to the results reported in section 4.1, it is clear that the current alignment configuration allows a much stronger stabilisation of the closed ring structures with vertical alignment. When the patterned rings at both substrates perfectly overlap, the defect-free director configuration with out-of-plane reorientation of the director (Figure 14(a-c)) is the only stable configuration and no alternative structures with twist disclinations appear. Remarkably, this conclusion still holds when the alignment patterns at the top and bottom substrate are substantially shifted (Figure 14(d-f)). The created topological solitons are precisely localised thanks to the substrate patterning and adjustments of the alignment patterns can tweak the bulk properties of the LC and therefore also the optical properties of the device. This offers interesting opportunities for different electro-optic applications and one domain that specifically attracts our attention is the manipulation of light. Strong interaction between light and the localised soliton structure (with large refractive index contrast) is expected and the interaction can be easily adjusted by applying low-voltage fields or other external stimuli. Due to the absence of in-plane rotational symmetry in the studied configuration, a very rich behaviour (including light deflection, polarisation conversion, etc.) can be foreseen, and this should be investigated further.

Recently we also investigated ring-shaped alignment patterns with two times 180° (at both substrates) or 360° (at one substrate) azimuthal rotation in combination with a radial or concentric background for $r < r_{in}$ and $r > r_{out}$, instead of a uniform background. This work, with rotational symmetry of the alignment pattern, is currently under review.

5. Conclusion

Combining orientationally patterned anchoring at two confining substrates with (chiral) nematic LC often leads to interesting three-dimensional LC superstructures in the bulk of the cell. Many different flat optical components with large optical efficiency and varied functionality have been developed in this way and often external stimuli such as an applied electric field can be used to tune the device characteristics. The bulk director configuration however may become very complex, especially when chiral LC or different anchoring patterns at the top and bottom substrates are used. Simulations are therefore often indispensable when a detailed knowledge of the director configuration is required. In this review, we give an overview of how different (periodic and non-periodic) azimuthal alignment patterns influence the self-assembly of NLC and CLC structures, based on the comparison between experimental results and simulations. Clear links between experiments with different alignment configurations are indicated to provide intuitive insight into the LC elastic behaviour between azimuthally patterned substrates. We explain why a slanted CLC configuration without defects but with a tilted helical axis can form on top of a rotating azimuthal alignment pattern (section 2). We also demonstrate for different examples that a twist conflict at the top and bottom substrate in NLC cells can often be resolved without the formation of disclinations by introducing an out-of-plane reorientation of the director in the bulk. This is, for example, the case for the electrically tunable 2D diffraction gratings discussed in section 3 and for the localised topological solitons in NLC cells without strong confinement or CLC discussed in section 4. In general, this research domain, investigating the effect of patterned anchoring on the bulk LC configuration, is still largely unexplored and different possibilities for future research have been indicated.

Acknowledgements

The author is very grateful to Prof. Kristiaan Neyts (Liquid Crystals and Photonics Group, Ghent University) for many topical and intellectual discussions about the research.

Disclosure statement

The authors declare no conflict of interest.

ORCID

Inge Nys http://orcid.org/0000-0001-8191-8128

References

[1] Woltman SJ, Jay GD, Crawford GP. Liquid-crystal materials find a new order in biomedical applications. Nat Matter. 2007;6:929–938.
[2] Beeckman J, Neyts K, Vanbrabant PJM. Liquid-crystal photonic applications. Opt Eng. 2011;50:081202.
[3] Lagerwall JPF, Scalia G. A new era for liquid crystal research: applications of liquid crystals in soft matter nano-, bio- and microtechnology. Curr Appl Phys. 2012;12:1387–1412.
[4] Schadt M. Liquid crystal displays, LC-materials and LPP photo-alignment. Mol Cryst Liq Cryst. 2017;647:253–268.
[5] Marrucci L, Manzo C, Paparo D. Pancharatnam-berry phase optical elements for wave front shaping in the visible domain: switchable helical mode generation. Appl Phys Lett. 2006;88:1–4.
[6] Chen P, Lu YQ, Hu W. Beam shaping via photopatterned liquid crystals. Liq Cryst. 2016;43:2051–2061.
[7] Miskiewicz MN, Escuti MJ. Optimization of direct-write polarization gratings. Opt Eng. 2015;54:025101.
[8] Kawai K, Sakamoto M, Noda K, et al. Three-dimensionally modulated anisotropic structure for diffractive optical elements created by one-step three-beam polarization holographic photoalignment. J Appl Phys. 2016;119:123102.
[9] Provenzano C, Pagliusi P, Cipparrone G. Electrically tunable two-dimensional liquid crystals gratings induced by polarization holography. Opt Express. 2007;15:5872–5878.
[10] Crawford GP, Eakin JN, Radcliffe MD, et al. Liquid-crystal diffraction gratings using polarization holography alignment techniques. J Appl Phys. 2005;98:1231021.
[11] Nys I, Beeckman J, Neyts K. Switchable 3D liquid crystal grating generated by periodic photo-alignment on both substrates. Soft Matter. 2015;11(39):7802–7808.
[12] Nys I, Nersesyan V, Beeckman J, et al. Complex liquid crystal superstructures induced by periodic photo-alignment at top and bottom substrate. Soft Matter. 2018;14(33):6892–6902.
[13] Nersesyan V, Nys I, Van Acker F, et al. Observation of symmetry breaking in photoalignment-induced periodic 3D LC structures. J Mol Liq. 2020;306:112864.
[14] Wang M, Li Y, Yokoyama H. Artificial web of disclination lines in nematic liquid crystals. Nat Commun. 2017;8:3881–3887.
[15] Zeng H, Wani OM, Wasylczyk P, et al. Self-regulating iris based on light-actuated liquid crystal elastomer. Adv Mater. 2017;29:1–7.
[16] Babakhanova G, Turiv T, Guo Y, et al. Liquid crystal elastomer coatings with programmed response of surface profile. Nat Commun. 2018;9:456.
[17] Kawai K, Sakamoto M, Noda K, et al. Tunable dichroic polarization beam splitter created by one-step

holographic photoalignment using four-beam polarization interferometry. J Appl Phys. 2017;121:013102.
[18] Chen P, Wei BY, Hu W, et al. Liquid-crystal-mediated geometric phase: from transmissive to broadband reflective planar optics. Adv Mater. 2019;32(27):19036651.
[19] Kobashi J, Yoshida H, Ozaki M. Planar optics with patterned chiral liquid crystals. Nat Photon. 2016;10:389–392.
[20] Xiang X, Kim J, Komanduri R, et al. Nanoscale liquid crystal polymer bragg polarization gratings. Opt Express. 2017;25:19298–19308.
[21] Chen H, Weng Y, Xu D, et al. Beam steering for virtual/augmented reality displays with a cycloidal diffractive waveplate. Opt Express. 2016;24:7287.
[22] Oh C, Escuti MJ. Achromatic diffraction from polarization gratings with high efficiency. Opt Lett. 2008;33:2287–2289.
[23] Gou F, Chen H, Li MC, et al. Submillisecond-response liquid crystal for high-resolution virtual reality displays. Opt Express. 2017;25(7):7984–7997.
[24] Li Y, Zhan T, Wu ST. Flat cholesteric liquid crystal polymeric lens with low f-number. Opt Express. 2020;28(4):5875–5882.
[25] Tabiryan N, Roberts D, Steeves D, et al. New 4G optics technology extends limits to the extremes. Photonics Spectra. 2017. https://www.photonics.com/Articles/New_4G_Optics_Technology_Extends_Limits_to_the/a61612
[26] Xiang X, Kim J, Escuti MJ. Bragg polarization gratings for wide angular bandwidth and high efficiency at steep deflection angles. Sci Rep. 2018;8(1):10–15.
[27] Gao K, McGinty C, Payson H, et al. High-efficiency large-angle pancharatnam phase deflector based on dual-twist design. Opt Express. 2017;25(6):6283–6293.
[28] Ozaki R, Hashimura S, Yudate S, et al. Optical properties of selective diffraction from bragg-berry cholesteric liquid crystal deflectors. OSA Continuum. 2019;2:3554–3563.
[29] Cho S, Yoshida H, Ozaki M. Emission direction-tunable liquid crystal laser. Adv Opt Mater. 2020;8:2000375.
[30] Xiang X, Escuti MJ. Numerical analysis of bragg polarization gratings. J Opt Soc Am B. 2019;36:D1–D8.
[31] Honma M, Nose T. Polarization-independent liquid crystal grating fabricated by microrubbing process. Jpn J Appl Phys. 2003;42:6992–6997.
[32] Nys I, Beeckman J, Neyts K. Surface-mediated alignment of long pitch chiral nematic liquid crystal structures. Adv Opt Mater. 2018;6:1800070.
[33] Nys I, Beeckman J, Neyts K. Voltage-controlled formation of short pitch chiral liquid crystal structures based on high-resolution surface topography. Opt Express. 2019;27(8):11492–11502.
[34] Kasyanova IV, Gorkunov MV, Artemov VV, et al. Liquid crystal metasurfaces on micropatterned polymer substrates. Opt Express. 2018;26(16):20258–20269.
[35] Prompinit P, Achalkumar AS, Bramble JP, et al. Controlling liquid crystal alignment using photocleavable cyanobiphenyl self-assembled monolayers. Appl Mater Inter. 2010;2(12):3686–3692.
[36] Yaroshchuk O, Reznikov Y. Photoalignment of liquid crystals: basics and current trends. J Mater Chem. 2012;22:286.
[37] Chigrinov V. Photoaligning and photopatterning — a new challenge in liquid crystal photonics. Crystals. 2013;3:149–162.
[38] Park S, Padeste C, Schift H, et al. Chemical nanopatterns via nanoimprint lithography for simultaneous control over azimuthal and polar alignment of liquid crystals. Adv Mater. 2005;17:1398.
[39] Komitov GP, Bryan-Brown EL, Wood ABJ, et al. Alignment of cholesteric liquid crystals using periodic anchoring. Appl Phys. 1999;86:3508–3511.
[40] Chen WZ, Tsai YT, Lin TH. Photoalignment effect in a liquid-crystal film doped with nanoparticles and azo-dye. Appl Phys Lett. 2009;94:201114.
[41] Nys I, Chen K, Beeckman J, et al. Periodic planar-homeotropic anchoring realized by photoalignment for stabilization of chiral superstructures. Adv Opt Mater. 2018;6(6):1701163.
[42] Berreman DW. Alignment of liquid crystals by grooved surfaces. Mol Cryst Liq Cryst. 1973;23:215.
[43] Takahashi H, Sakamoto T, Okada H. Liquid crystal device with 50 nm nanogroove structure fabricated by nanoimprint lithography. J Appl Phys. 2010;108:113529.
[44] Wahle M, Brassat K, Ebel J, et al. Two-dimensional switchable blue phase gratings manufactured by nanosphere lithography. Opt Express. 2017;25:59–65.
[45] Berteloot B, Nys I, Poy G, et al. Ring-shaped liquid crystal structures through patterned planar photo-alignment. Soft Matter. 2020;16(21):4999–5008.
[46] Guo Y, Jiang M, Peng C, et al. High-resolution and high-throughput plasmonic photopatterning of complex molecular orientations in liquid crystals. Adv Mater. 2016;28:2353–2358.
[47] Kim J, Li Y, Miskiewicz MN, et al. Fabrication of ideal geometric-phase holograms with arbitrary wavefronts. Optica. 2015;2:958.
[48] De Sio L, Roberts D, Liao Z, et al. Digital polarization holography advancing geometrical phase optics. Opt Express. 2016;24(16):18297–18306.
[49] Provenzano C, Pagliusi P, Cipparrone G. Highly efficient liquid crystal based diffraction grating induced by polarization holograms at the aligning surfaces. Appl Phys Lett. 2006;89:121105.
[50] Duan W, Chen P, Wei BY, et al. Fast-response and high-efficiency optical switch based on dual-frequency liquid crystal polarization grating. Opt Mater Express. 2016;6:597–602.
[51] Ma Y, Tam AMW, Gan XT, et al. Fast switching ferroelectric liquid crystal pancharatnam-berry lens. Opt Express. 2019;27(7):10079–10086.
[52] Tervo J, Turunen J. Paraxial-domain diffractive elements with 100% efficiency based on polarization gratings. Opt Lett. 2000;25:785–786.
[53] Escuti MJ, Jones WM Polarization independent switching with high contrast from a liquid crystal polarization grating. SID International Symposium, Seminar, and Exhibition, San Francisco, CA. 2006;37:1443.
[54] Pancharatnam S. Generalized theory of interference, and its applications. coherent pencils. Proc Indian Acad Sci Sect A. 1956;44:247-262.
[55] Berry MV. Diabolical points in the spectra of triangles. Proc R Soc London Ser A. 1984;392:15-43.
[56] Komanduri RK, Escuti MJ. Elastic continuum analysis of the liquid crystal polarization grating. Phys Rev. 2007;76:0217011.

[57] Nys I, Stebryte M, YYe U, et al. Tilted chiral liquid crystal gratings for efficient large-angle diffraction. Adv Opt Mater. 2019;7(22):1901364.
[58] Stebryte M, Nys I, Ussembayev YYE, et al. Large angle forward diffraction by chiral liquid crystal gratings with inclined helical axis. Crystals. 2020;10:8071.
[59] Lee YH, Yin K, Wu ST. Reflective polarization volume gratings for high efficiency waveguide-coupling augmented reality displays. Opt Express. 2017;25:27008–27014.
[60] Weng Y, Zhang Y, Cui J, et al. Liquid-crystal-based polarization volume grating applied for full-color waveguide displays. Opt Lett. 2018;43:5773–5776.
[61] Lee YH, He Z, Wu ST. Optical properties of reflective liquid crystal polarization volume gratings. J Opt Soc Am B. 2019;36:D9–D12.
[62] Xiang J, Shiyanovskii SV, Imrie CT, et al. Electrooptic response of chiral nematic liquid crystals with oblique helicoidal director. Phys Rev Lett. 2014;112:217801.
[63] Iadlovska OS, Maxwell GR, Babakhanova G, et al. Tuning selective reflection of light by surface anchoring in cholesteric cells with oblique helicoidal structures. Opt Lett. 2018;43:1850–1853.
[64] Sunami K, Imamura K, Ouchi T, et al. Shape control of surface-stabilized disclination loops in nematic liquid crystals. Phys Rev E. 2017;97(2):020701.
[65] Nys I, Berteloot B, Poy G. Surface stabilized topological solitons in nematic liquid crystals. Crystals. 2020;10(9):840.
[66] Honma M, Toyoshima W, Nose T. Bistable liquid crystal device fabricated via microscale liquid crystal alignment. J Appl Phys. 2016;120:143105.
[67] Ouchi T, Imamura K, Sunami K, et al. Topologically protected generation of stable wall loops in nematic liquid crystals. Phys Rev Lett. 2019;123:097801.
[68] Smalyukh II, Lansac Y, Clark NA, et al. Three-dimensional structure and multistable optical switching of triple-twisted particle-like excitations in anisotropic fluids. Nat Mater. 2010;9:139–145.
[69] Loussert C, Brasselet E. Multiple chiral topological states in liquid crystals from unstructured light beams. Appl Phys Lett. 2014;104:051911.
[70] Tai JSB, Smalyukh II. Surface anchoring as a control parameter for stabilizing torons, skyrmions, twisted walls, fingers and their hybrids in chiral nematics. Phys Rev E. 2020;101:042702.